

Received 27 May 2022; revised 8 September 2022 and 21 October 2022; accepted 4 November 2022. Date of publication 21 November 2022; date of current version 29 November 2022.

Digital Object Identifier 10.1109/OJUFFC.2022.3221708

Scandium-Doped Aluminum Nitride PMUT Arrays for Wireless Ultrasonic Powering of Implantables

BERNARD HERRERA[®] (Member, IEEE), PIETRO SIMEONI[®] (Member, IEEE), GABRIEL GIRIBALDI[®] (Student Member, IEEE), LUCA COLOMBO[®] (Member, IEEE), AND MATTEO RINALDI[®] (Senior Member, IEEE)

Northeastern SMART Center, Department of Electrical and Computer Engineering, Northeastern University, Boston, MA 02118 USA CORRESPONDING AUTHOR: B. HERRERA (herrerasoukup.b@northeastern.edu)

This work was supported by the Defense Advanced Research Projects Agency (DARPA) TUnable FErroelectric Nitrides (TUFEN)
Program under Grant HR00112090045.

ABSTRACT The present work reports on the novel usage of Scandium-doped Aluminum Nitride (AlScN) PMUT arrays for enhanced power transfer in implantable applications. Optimization considerations were explored for the PMUT array towards high performance. The transmission metric, compared to identical arrays based on Aluminum Nitride (AlN), showed a 25dB increase. Power transfer measurements also confirmed a considerable increase as compared to previous work based on AlN. Different matching strategies were explored to maximize the output power including inductor conjugate matching and matching utilizing resonators in series and parallel topologies. A full characterization of the transferred power versus incident acoustic intensity on the array revealed transmission of power levels of several milliwatts for intensities below the Food and Drug Administration's (FDA) limit. The performance of the array, as compared with other implementations with a range of frequencies, dimensions and input acoustic intensities was bench-marked through the use of the conversion efficiency as the figure-of-merit. The practical applicability of the system, utilizing a realistic tissue phantom as the medium, was proven by interfacing with a commercially available boost converter to obtain a rectified voltage and power levels sufficient for powering and charging intra-body electronics.

INDEX TERMS PMUT, ultrasonic, intra-body, power transfer, scandium-doped aluminum nitride.

I. INTRODUCTION

SEVERAL technologies have been considered with the objective of wirelessly powering or recharging batteries in implantable electronic nodes [1]. As compared to other mechanisms, such as inductive, capacitive, and radiofrequency links, ultrasonic power transfer stands out due to the lower signal attenuation of ultrasonic waves in tissue and due to the relatively higher safety thresholds for allowable transmitted power.

Within ultrasonic power receivers, a fair amount of work has utilized bulk thickness-extensional mode transducers [2] resulting in high power outputs but having the caveat of being invasive due to their minimum dimensions required. A further step within these kind of transducers has been the demonstration of minute Lead Zirconate Titanate (PZT) cubes allowing to power implantable Application-Specific

Integrated Circuits (ASICs) for optogenetic stimulation [3], wireless recording of bio-signals [4], deep-tissue oxygenation monitoring [5] and bi-directional data links [6].

A different transduction mechanism, where a diaphragm structure is constructed based on a piezoelectric and a passive layer, allows for receivers with a flat form factor and increased acoustic impedance matching to liquid media. Such membrane receivers, based on Lead Zirconate Titanate (PZT) have also been explored in terms of their ultrasonic power transfer capabilities [7], [8].

Within this realm, AIN is an alternative, well established piezoelectric thin film material that offers higher biocompatibility, can be integrated in Complementary Metal-Oxide-Semiconductor (CMOS) processing, and allows for arrays of hundreds of devices to be fabricated in a miniature chip form factor, enabling beam-forming capabilities.

However, explorations on utilizing AlN PMUT arrays as power receivers have been limited [9].

AlN thin films, have also been the subject of recent research where Scandium doping of the crystal has shown considerable increases in the energy harvesting Figure-of-Merit ($FOM = e_{31,f}^2/\epsilon_r\epsilon_0$) along with the levels of Sc doping [10]. This is due to the film's significantly lower dielectric permittivity, despite its smaller piezoelectric coefficients, as compared to other piezoelectrics like PZT [11]. The use of Scandium doping in the piezoelectric layer of PMUTs has also been proven to offer improved performance, in terms of sensitivity, as compared to identical devices based on pure AlN [12], [13].

Common to all PMUTs, based on different piezoelectric materials, is the fact that the inevitable parallel plate structure for actuation results in a considerable static capacitance. This results in a significant amount of the available received power to become reactive. A common approach to mitigate this effect is to use inductors, cancelling out the reactance at the specific operating frequency. Recent work has demonstrated the potential of utilizing resonators to provide both this matching effect as well as voltage-boosting [14].

The present work therefore focuses on characterizing the power transfer capabilities of AlN PMUT arrays enhanced by scandium doping, further detailing and extending the work on a previous demonstration [15]. Design considerations are explored, a comparison of performance with and without Sc doping is performed and characterization of the power transfer capabilities is made for a range of input sound intensity levels. Furthermore, inductor and resonator-based matching approaches are compared. A practical demonstration is also showcased, transferring power across a tissue phantom and utilizing a commercially-available boost converter chip for rectification. The present work is therefore aimed at enabling AlScN PMUT arrays for the powering of Application Specific Integrated Circuits (ASICs) and the recharging of batteries in miniaturized implantable nodes for sensing and stimulation, with the possibility of CMOS integration and concurrent wide-band ultrasonic communication capabilities.

II. METHODOLOGY

A. PMUT ARRAY DESIGN

Given their topology, PMUTs have several parameters dictating their behaviour, and thus several degrees of freedom in their design. In order to narrow down the options, for the particular power transfer application, the first parameter that was set was the thickness of the piezoelectric layer. This thickness came from a perspective of ease of fabrication of a high quality film. Particularly for AlScN, a good film quality is more easily obtained after a certain thickness of the film [16], providing ample time for seeding of the crystal columns and proper alignment to take place during deposition. Thicker films usually improve the crystal quality but require longer deposition times, increasing the cost. A thickness of 500nm was chosen as a trade off between rocking curve and deposition time.

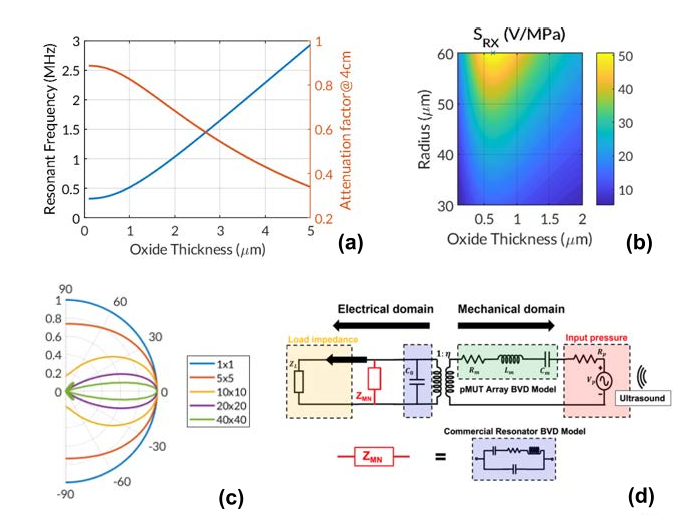


FIGURE 1. (a) Analytical resonant frequency and attenuation factor vs passive layer thickness. (b) Trend of PMUT receiving sensitivity S_{RX} for different combinations of cavity radius and elastic layer thickness. (c) Array directivity for different number of elements in the array. (d) Equivalent circuit modeling the acoustic, mechanical and electrical branches of the PMUT array and its interfacing with a resonator-based matching network and load.

The passive material to be used was chosen to be silicon dioxide (see section II-B). An analytical model for the resonant frequency of the devices was developed based on the equations in [17] and [18], where a flexural rigidity and neutral axis are first calculated dependent on the thicknesses, Young's modulii, and Poisson's ratios of the material stack. A resonant frequency in air is calculated based on those and a water loading factor is then introduced as described in [19]. Fig. 1,a) shows a sweep of the thickness of the passive layer and the resulting resonant frequencies and attenuation factor of the signal at a distance of 4cm. The results correspond to a fixed radius of $46\mu m$, which was selected as a Deep Reactive Ion Etching (DRIE) recipe was readily available from previous experience of the authors.

To gain insight on the dependence of the receiving sensitivity of the PMUTs with respect to the elastic layer thickness and radius, the model described in [20] was implemented to obtain the mechanical, electrical and acoustic parameters of the PMUT Modified Butterworth Van-Dyke (MBVD) equivalent circuit for different combinations of radii and oxide thicknesses. Table 1 details the relevant parameter utilized for the 36% Sc-doped AlN film only, as the parameters for the rest of materials are widely known. Finally, the S_{RX} equation from [21] was calculated and plotted in fig. 1,b).

An oxide thickness of $1\mu m$ was selected, due to readily available thermal oxide wafers with that thickness, along with the available $46\mu m$ radius process. The results suggest that the sensitivity can be further optimized with a slightly thinner oxide layer and larger cavity radius. However, larger membranes are more prone to bending and breakage as a result of residual stresses in high aspect ratio membranes.

TABLE 1. MBVD model parameters.

Symbol	Parameter	Value	Units
$e_{31,f}$	Transverse film piezo constant	2.6	C/m^2
ϵ_{33}	Dielectric constant	18.6	_
β	Water loading factor	0.669	_
Y_{AlScN}	Piezoelectric Young's Modulus	230	GPa
ν_{AlScN}	Piezoelectric Poisson's ratio	0.25	_

The resulting resonant frequency also constrains medium attenuation to an acceptable value.

Finally, array parameters were considered. A large number of elements, and a high fill factor, are desirable as the power generated by each element adds up to the total. However, as can be seen in Fig. 1,c), a higher number of elements also increases the array's directivity, making the beam narrower and making the power transfer system more susceptible to misalignment between transmitter and receiver. The directivity was calculated from the product of the single-element directivity, which depends on the ratio of the PMUT radius and wavelength, and the array directivity, which depends on the number of elements, wavelength and pitch as detailed in [22]. A pitch smaller than $\lambda/2$ was used in order to prevent sidelobes in the directivity response [23]. 20×20 elements, and a pitch of $180\mu m$ were parameters seen to offer an acceptable trade-off.

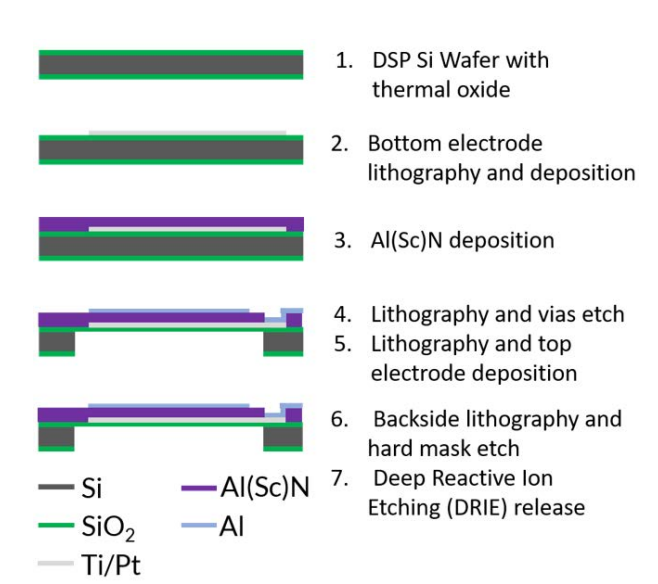


FIGURE 2. Schematic fabrication process flow for AI(Sc)N PMUTs.

B. FABRICATION

Figure 2 shows the steps involved in the fabrication of the PMUTs. 0 and 36% Sc-doped AlN PMUT arrays of 20×20 elements connected in parallel, with a radius of $46\mu m$, and a pitch of $180\mu m$ were micro-fabricated. The substrate used was a $300\mu m$ Double-Side Polished (DSP) silicon wafer with a $1\mu m$ thermal oxide (SiO_2) layer. A Ti adhesion layer of approximately 5nm was first deposited over which 150nm of

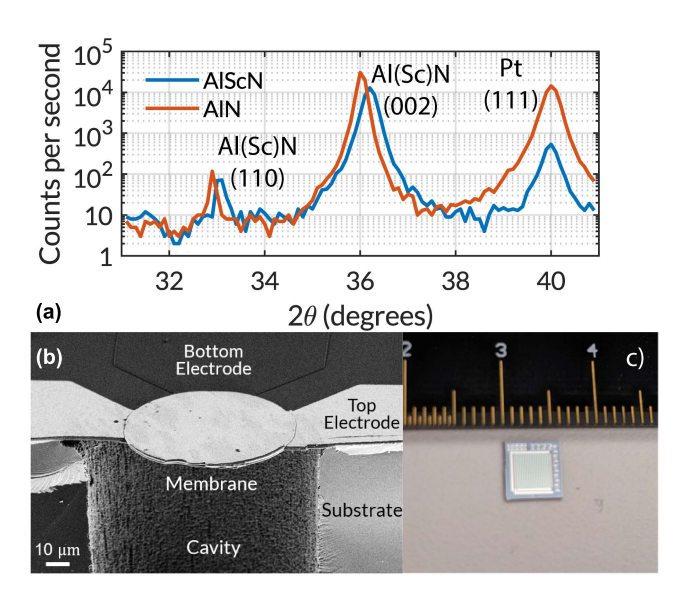


FIGURE 3. (a) XRD 2θ scan for the AIN films with and without Sc doping. The AI(Sc)N 002 peak is clearly evident. (b) SEM cross-section view of a PMUT element within the fabricated array. (c) Photograph of the fabricated chip before wirebonding and PDMS encapsulation.

Pt were sputtered as a bottom electrode. After patterning the bottom electrode through lift-off, the AlN layer was grown targeting 500nm. The two different piezoelectric layers were deposited using an Evatec Clusterline multi-target sputtering system. For the Sc-doped film, 900 W DC + 100 RF were applied to an Al target while applying 710 W to a Sc target in a nitrogen atmosphere. Vias were etched in phosphoric acid at $150^{\circ}C$. Finally, a 90nm Al layer was deposited and patterned via lift-off to serve as the top electrode.)

The existing thermal oxide layer on the backside of the wafer was then patterned into a hard mask through a photo-lithography process with back-side alignment and Reactive Ion Etching (RIE). Finally, the membranes were released via a through-wafer Deep Reactive Ion Etching (DRIE) process.

X-Ray Diffractometry (XRD) was performed on the metalpiezoelectric stack, particularly to verify the crystallinity of the AlScN layer. Full-Width Half Maximum (FWHM) rocking curve values of 2.1 for AlScN and 2.17 degrees for AlN, as well as clear 002 Al(Sc)N peaks verified the piezoelectric film quality (Fig. 3 a.). Scanning Electron Microscope (SEM) images of a fabricated device are shown in Fig. 3,b). while a photograph of the fabricated chip is shown in Fig. 3,c).

The two resulting chips were wire-bonded to dedicated Printed Circuit Boards (PCBs) with coaxial Sub-Miniature version A (SMA) cables for electrical routing and shielding from noise. The assembly was encapsulated in polydimethysiloxane (PDMS) for both electrical insulation as well as for mechanical protection of the delicate membranes. The elasticity of the polymer and its similar acoustic impedance to the one of aqueous media prevents it from significantly impacting the performance of the PMUT elements.

C. MATCHING NETWORKS

Due to their structure, based on a piezoelectric layer in between parallel conductors, PMUTs are characterized by a considerable static capacitance. This effect adds up linearly when combining multiple elements in parallel into an array. The presence of this considerable capacitance transforms a good portion of the power converted from the ultrasonic wave input into reactive power. The straightforward way to recover this input is to perform conjugate matching. That is, to connect an inductor in series with the array having an inductance value such that it cancels out the capacitive reactance. Such a matching will be intrinsically narrow-band, as there is only one frequency at which this cancelling occurs exactly. This does not pose a limitation, as power transfer does not require a wide band of operation. The sharpness of the matching peak in the system's admittance will, of course, depend on the quality factor (Q) of the inductor. Lower quality factors will introduce additional losses that reduce the effectiveness of the approach.

For the inductance values and frequencies of operation required to match the capacitance of a typical PMUT array useful for liquid media power transfer applications, the quality factor of commercially available inductors tends to be poor, as compared with components for higher frequency RF applications. The lower frequency of operation is desirable to minimize attenuation of the ultrasonic wave in the medium. The size of the inductors also becomes considerable at the required values of inductance, especially when considering that one of the advantage of utilizing PMUT arrays is their capability of miniaturization for potential implantable applications.

A potential solution comes from the use of piezoelectric resonators which can have very high quality factors and, especially if utilizing MEMS resonators, can have miniature form factors and be potentially integrated into the PMUT fabrication process flow. In recent works, MEMS resonators have been utilized to provide passive gains on capacitive loads in RF circuits [24], [25] and the concept has also been applied to increase the receive and transmit sensitivity of PMUT arrays through a voltage-boosting effect [14], [26]. In a similar manner, resonators can potentially be utilized to improve the extracted power from a PMUT array by cancelling out the capacitive reactance. This is due to the fact that, in between resonance and antiresonance, the reactance of the resonator has a very wide swing and it will cancel out the capacitance at a specific frequency.

The power transfer capabilities of the bare PMUT array and of the array interfaced with an inductor and with resonators in parallel and series configurations are thus investigated in this work.

D. MEASUREMENT SETUP

Figure 4 schematically summarizes the different test setups used for characterization of the PMUT arrays response and the different matching networks considered.

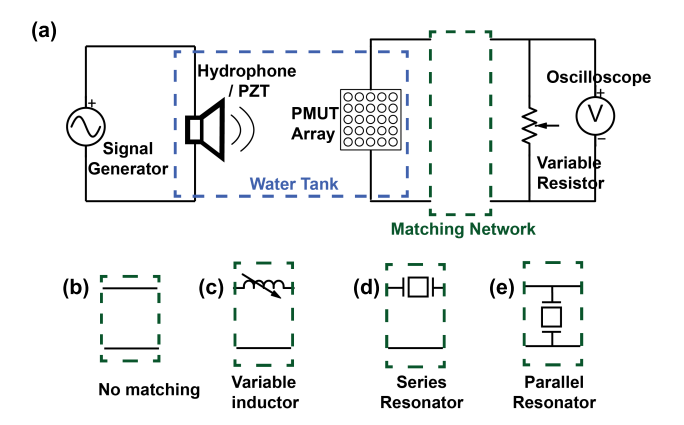


FIGURE 4. (a) Schematic of the generalized test setup. (b) No matching network. Used for AIN vs AIScN array comparison and load optimization with no matching network. (c) Conjugate matching. (d) Series resonator. (e) Parallel resonator.

First, the frequency response of the acoustic transmission was characterized by impulse response measurements from a wide-band reference hydrophone (Teledyne Reson TC 4038) to both the PMUT arrays. Transmission between two identical AlScN arrays was also measured and the experiment was repeated between two identical AlN arrays. The measurement was performed with both the transmitter and receiver elements submerged in De-Ionized (DI) water.

Once the superior performance of the AlScN against the AlN array was verified, only the former was utilized in the rest of the experiments. The admittance of the submerged array was measured through a Vector Network Analyzer (VNA) and a Thevenin's equivalent for its source impedance, at resonance, was obtained.

Load resistance optimization and conjugate matching of the device's static capacitance were later performed. A Commercial Off-The-Shelf (COTS) bulk PZT transmitter, with a 700 kHz resonance frequency, was used as a transmitter. The PMUT array was placed facing the transmitter at a distance of 4cm in water. A $10V_{pp}$, 10 cycle tone-burst was applied to the PZT to prevent standing wave effects and to avoid capacitive coupling, which appears simultaneously with the applied burst, to merge with the acoustic signal that appears after the sound propagation delay. The output voltage was measured on a variable resistance connected in parallel with the PMUT array. The experiment was then repeated by placing a matching inductor in series with the load resistance. The inductance was calculated as the conjugate of the measured reactance of the PMUT array at the operating frequency (dominated by the static capacitance C_0).

Utilizing the same setup, the experiment was repeated by replacing the inductor with a COTS resonator in series with the PMUT array. The parallel configuration was also tested in which the array, resonator and load resistance are all in parallel.

Characterization of the output power and conversion efficiency was performed for varying incident acoustic

intensities on the array surface. The voltage on the transmitting PZT was varied by using an ultrasonic pulser and a reference hydrophone measured the acoustic pressure at the location were the PMUT array would be located. Then, after placing the array back as a receiver, the output power on the load was measured and power and efficiency were calculated.

Finally, the optimized receiver was interfaced to an EM8900 boost converter [27] to obtain a rectified voltage in two experiments involving 4cm of water and 6cm of tissue phantom, respectively.

Common to all the different testing setups used is the fact that, since the distance between the receiver (4cm) and the PZT transducer is larger than the wavelength, the transmission will be considered far-field and the propagating waves will have a spherical distribution. This could result in the different elements within the PMUT array to be hit by the wavefront with a certain delay between each other. Then, the amplitude of the output voltage of the array could not be simply assumed to be the number of elements times the output of each element and the signal could be distorted. Also, for simulation purposes, the acoustic wave source in circuits would not be a single anymore but rather should be modeled as several sources phase-shifted respect to each other.

Therefore, a COMSOL FEM simulation was run of the acoustic pressure field between the PZT transducer source and the PMUT array. An axisymmetric 2D simulation of half of the domain was used to reduce computational cost. The phase of the acoustic wave was extracted at the face of the PMUT array. As seen in figure 5, the maximum phase shift obtained is six degrees, which can be considered negligible.

III. RESULTS

A. EFFECT OF SCANDIUM DOPING

Fig. 6 details the impulse response as well as the corresponding Fast Fourier Transform (FFT) for transmission from a reference hydrophone to the AlN and to the AlScN PMUT arrays. The transmission between two identical AlScN arrays was also measured, while the Signal-to-Noise (SNR) level for a similar link between two AlN arrays was too low for direct measurement.

From the measurements, the improved performance of the AlScN PMUTs is evident. An increase of 25 dB can be observed at the center frequency. The measured bandwidth also appears to be larger. However, even though the hydrophone is relatively wideband, it does introduce a pass band response of its own. Therefore, the measurement between the two AlScN arrays gives a better assessment of the bandwidth. The large resulting value can be of interest for high data rate ultrasonic communication, another interesting feature offered by PMUT arrays due to their inherently good acoustic matching to liquids.

B. LOAD OPTIMIZATION AND INDUCTOR MATCHING

Fig. 7 details the load resistance sweeps for the output power with and without the matching inductor. For both cases,

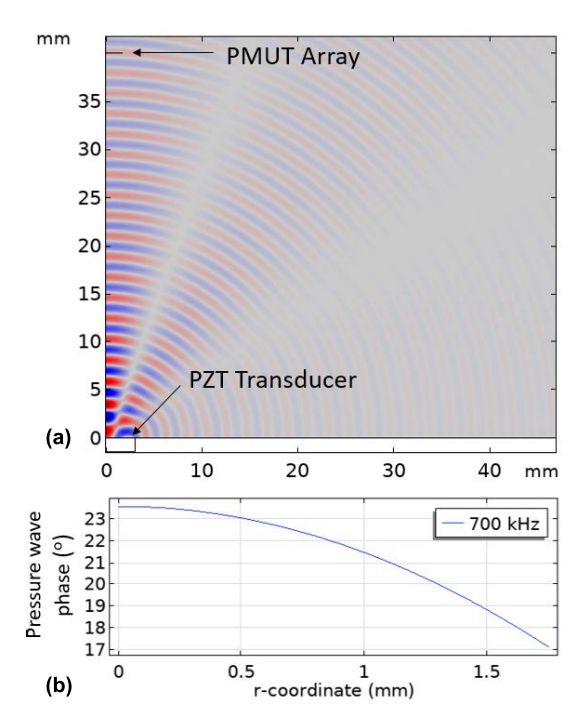


FIGURE 5. (a) 2D FEM simulation of teh acoustic pressure field between the PZT source transducer and the receiver PMUT array. (b) Phase of the acoustic wave along the length of the array verifying a negligible phase shift across the elements.

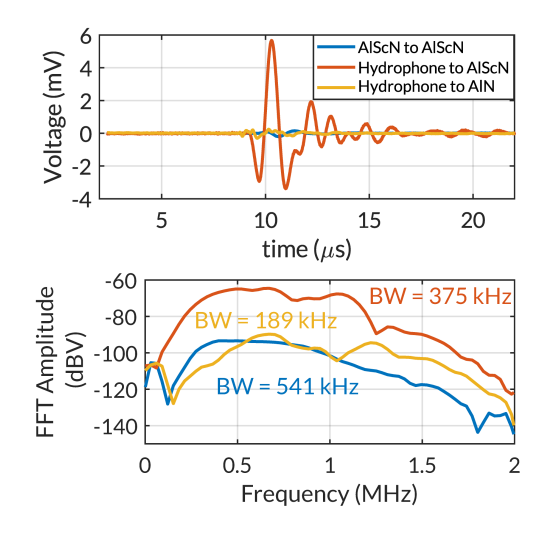


FIGURE 6. Impulse response (top) and frequency spectrum (bottom) for the acoustic transmission in water for AIN and AIScN arrays.

a maximum in the transferred power is observed, consistent with the maximum power transfer theorem. A $95.6\mu H$ inductor was used, corresponding to the conjugate of the reactance of the PMUT array at resonance.

For the case with no matching, the maximum occurs at approximately 400Ω , which coincides with the absolute value of the sum of the array's source resistance and the reactance due to C_0 . For the matched case, the optimal load is much

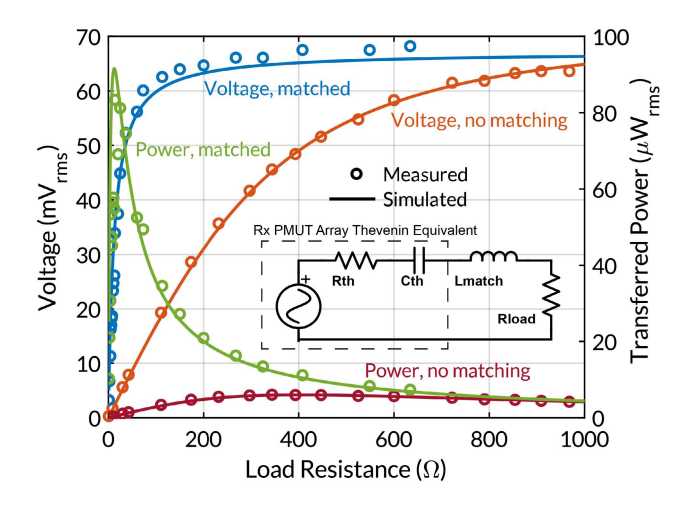


FIGURE 7. Measured and simulated values for the power transfer load optimization. The cases with and without a conjugate matching inductor are depicted. Acoustic intensity on the face of the array: 7mW/cm². Inset: Schematic of the circuit including the receiver PMUT array Thevenin's equivalent, matching inductor and load resistance.

smaller, as the contribution of the reactance has been resonated out by the added inductance. The output power is also increased by a factor of 14 due to the elimination of the reactive power.

When the array acts as a receiver, the transduction of the incident pressure to charge across the PMUT electrodes can be basically modeled as a current source in parallel with the array's static capacitance C_0 . A resistance must also be added, accounting for the combination of the electrical trace resistance R_0 and the mechanical resistance R_m , as described in the Modified Butterworth Van Dyke (MBVD) model. Since the array is operated at resonance, the other motional terms (C_m and L_m) cancel each other out. In order to see the circuit more clearly, in terms of the maximum power transfer theorem, it is desirable to convert this circuit to a voltage source in series with a source impedance. This can be done through a Thevenin's equivalent circuit.

Following this logic, from the impedance of the array measured with the VNA, calculations were performed for conversion to a Thevenin's equivalent. The circuit was implemented in Keysight's Advanced Design System (ADS) circuit simulator along with a load resistance. When this resistance was swept, the resulting simulated output power to the load matched the resistance sweep measurements closely, for both the cases with and without the matching inductor.

C. RESONATOR MATCHING

Fig. 8 details the results for the case of the resonator connected in parallel with the load. Measured results were compared with a circuit simulation performed in Keysight's Advanced Design System (ADS). Modified Butterworth Van-Dyke (MBVD) circuit parameters, for a single PMUT element, were obtained from an analytical model as detailed

TABLE 2. Resonator fitting parameters.

Symbol	Parameter	Value	Units
\overline{Q}	Quality factor	1590	_
k_t^2	Electromechanical Coupling	14.6	%
$ {C_0}$	Static Capacitance	191	pF
R_0	Dielectric Loss Resistance	1.19	$M\Omega$
R_s	Trace electrical Resistance	0.65	Ω
R_m	Mechanical Resistance	6.9	Ω
$\underline{\hspace{1cm}}f_s$	Resonant Frequency	587	kHz

in [28]. The individual PMUT model was encapsulated in a cell and groups of these cells were combined to model the 20×20 array. The input pressure to the array corresponded with the value measured with the reference hydrophone placed at the same location where the PMUT array is later placed. As for the resonator, the MBVD parameters were obtained from a fitting of admittance measurements obtained using a Vector Network Analyzer (VNA). The relevant parameters are shown in table 2.

Fig. 8 illustrates the obtained results. The top portion corresponds to a frequency sweep of the voltage across the load for varying values of its resistance. A clear peak is observed around the series resonance frequency of the resonator, particularly for high values of the load impedance. The magnitude of the voltage at this peak is approximately one order of magnitude higher as compared to the values from Fig. 7, consistent with the expected voltage boosting effect. As the load resistance decreases, it lowers the quality factor of the network and the voltage boosting effect is diminished.

The bottom portion of Fig. 8 shows the results for the load optimization at the system's resonant frequency obtained from the previous frequency sweep. The optimal power is obtained at a 5.21 $k\Omega$ load. Even though the maximum power transferred falls shy of the value obtained with inductor matching in section III-B, it is higher than the value with no matching and the considerably higher voltage obtained could enable direct rectification without the need of further boost converter circuitry (see section III-E).

Similarly, Fig. 9 details the frequency sweep and load resistance optimization results, in the top and bottom portions respectively, for the resonator connected in series between the PMUT array and the load. In this case, the voltage boosting effect is still present but occurs across the series connection of the resonator and load. Therefore, the load voltage itself is lower than the one attainable with the parallel connection. The maximum power level attained is comparable, but at a lower optimal load of 21Ω .

For both the results of series and parallel connections, a slightly higher mismatch is observed between measured and simulated results. This can be attributed to the fact that the variable resistor used as a load has different parasitic capacitance values for each resistance. These parasitics influence the resonant frequency, which has to be adjusted for maximum voltage amplitude, which is not done on the ADS simulation.

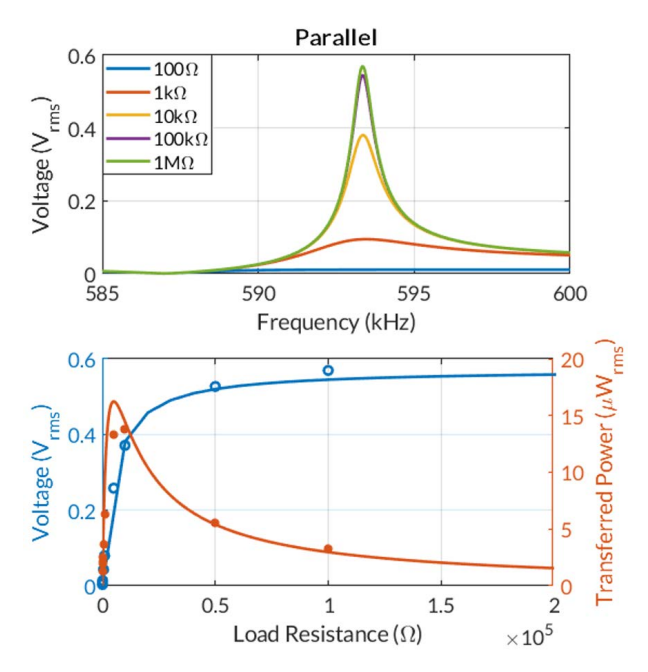


FIGURE 8. Parallel Resonator Configuration. Top: Frequency sweep of voltage on load for different load values. Bottom: Load optimization for power transfer.

It should be mentioned that, since the resonator will be packaged and isolated from the medium in the final application, it's resonant frequency and quality factor should not change due to contact with the medium. All the measurements described were taken at room temperature. Variations in the temperature of the medium could change the PMUT's resonant frequency should slightly due to the stiffness change of the material. The resonator's center frequency is not expected to change as it should be isolated form the medium and because resonators usually have relatively small Temperature Coefficients of Frequency (TCFs). Since the PMUTs in water have a broad bandwidth, the frequency of maximum voltage of the system will depend mainly on the resonant frequency of the resonator, and this variation is expected to be small.

In relation to the quality factor of the resonator, [14] details circuit simulations of the impact of the resonator's Q on the receiving voltage sensitivity. It was found to be proportional to this parameter. The main energy loss mechanisms for the resonator are electrical losses (tan delta), mechanical dissipation and energy losses to the packaging. Thus, improvement of this parameters and the use of MEMS resonators could further enhance sensitivity and allow for further miniaturization.

D. POWER TRANSFER EFFICIENCY

Fig. 10 details the output power and transfer efficiency for the matched and un-matched cases for varying incident sound intensities on the face of the PMUT array. The conversion efficiency is defined as the ratio of the output electrical power on the optimal load to the input sound intensity, on the face of the receiver, multiplied by the array's active area.

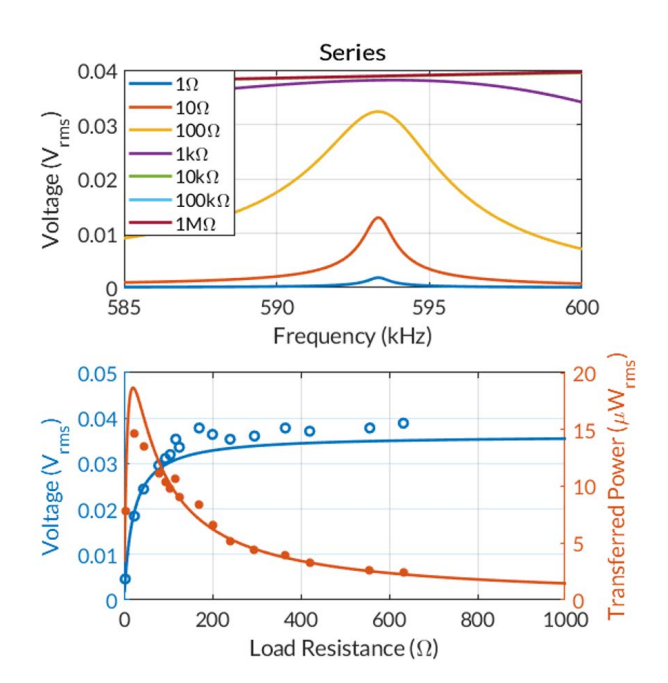


FIGURE 9. Series Resonator Configuration. Top: Frequency sweep of voltage on load for different load values. Bottom: Load optimization for power transfer.

This conversion efficiency is independent on the transmitter characteristics and attenuation in the medium at the particular distance of measurement. Thus, it serves to characterize the performance of the receiver only. As defined in [29] and [30], this conversion efficiency depends on the product of several individual efficiencies. The relevant ones, for this particular measurement setup, are:

$$\eta_{total} = \eta_{aperture} \eta_{match} D_a \tag{1}$$

$$\eta_{total} = \eta_{aperture} \eta_{match} D_{a} \tag{1}$$

$$\eta_{aperture} = \frac{S_{RX}^{2} Z_{0}}{4R_{transducer} A_{physical}} \tag{2}$$

$$\eta_{match} = \frac{R_{load}}{R_{load} + R_{PMUT}} \tag{3}$$

$$\eta_{match} = \frac{R_{load}}{R_{load} + R_{PMIT}} \tag{3}$$

where $\eta_{aperture}$ captures the conversion of incident acoustic power to available electrical power. Since the resistance of the transducer $R_{transducer}$ is taken into account, which includes the radiation resistance of the array, as well as its physical area $A_{physical}$, and the acoustic impedance of the medium Z_0 , this aperture efficiency models the relation of the transducer size relative to the wavelength of operation. This is very similar to the concept of effective aperture versus physical size in Radio Frequency (RF) antennae. The sensitivity in receive mode, S_{RX} captures the electromechanical conversion itself. For the particular setup in this work, $S_{RX} = 6mV/kPa$ and $R_{transducer} = 13.8$ which results in $\eta_{aperture} = 0.38$.

 D_a , the diffraction constant ([23] section 4.6, page 198), takes into account the interactions of reflections from the receiver itself, which can be significant for planar transducer arrays larger than the wavelength and can be approximated to 2 for this case [23]. Finally, η_{match} is dependent

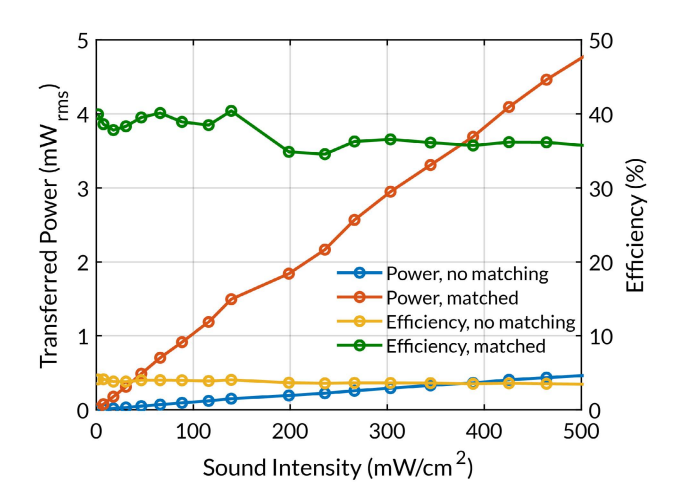


FIGURE 10. Transferred power to the load and conversion efficiency, with and without matching, for varying levels of sound intensity on the face of the PMUT array.

on the matching of the load and source resistances. For the maximum power transfer, the efficiency attainable is 0.5, according to the Maximum Power Transfer Theorem for the source-load resistor divider configuration. Thus, $\eta_{total} = 0.38$, which matches the measured efficiency.

It is important to highlight that the reported quantities are Root-Mean-Square values, as is standard for power measurements and it allows for correct comparison with the FDA's limit on Spatial-Peak-Temporal-Average Intensity (I_{SPTA}) sound intensity of $720mW/cm^2$. The transferred power values reported in Fig. 10 correspond to sound intensity values below the threshold.

E. VOLTAGE RECTIFICATION

Finally, the power transfer system was put to the test in a more practical application involving generating a rectified voltage output that can be utilized for powering ASICs. Fig. 11 shows the utilized test setup for the case of transmission through a tissue phantom mimicking the intra-body conditions.

Fig. 12 depicts the schematic of the test setup including the interfacing of the PMUT array, through the matching inductor, to the transformer required both for voltage amplification and for the inductive boost-converter of the EM8900 chip.

The output storage capacitor is included as well as intermediate capacitors for filtering and storage as recommended by the supplier. It is worthwhile to mention that the low input impedance of the boost converter circuit matches well with the reduced source impedance of the PMUT array after conjugate matching.

After a rise time, corresponding to the boost converter operation, steady states values of 1.8 and 1 V were obtained for links at distances of 4cm in water and 6cm in tissue phantom media at input acoustic intensities of 30.5 and 32.5 mW/cm^2 respectively.

The EM8900 chip performs the boost conversion only, but can be interfaced to further power management Integrated



FIGURE 11. Photograph of the test setup for power transfer from a COTS bulk PZT transmitter to the AISCN PMUT array through a tissue phantom. Included are the conjugate matching inductor and boost converter circuit for voltage conditioning and rectification.

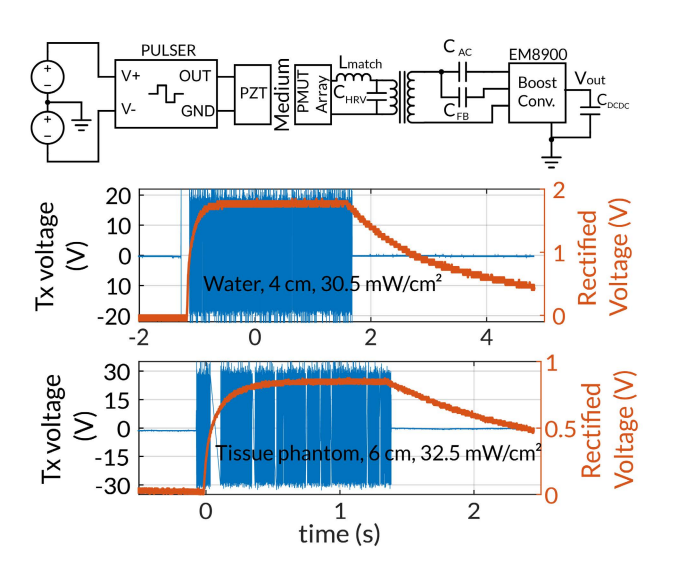


FIGURE 12. Top: Schematic of the test setup for power transfer and voltage rectification through a tissue phantom. Transient response of the voltage applied to the transmitting PZT transducer and the output rectified voltage for the experiments in water (center) and the tissue phantom (bottom).

Circuits (ICs), such as the EM8502 [31]. Such an IC integrates Low Dropout (LDO) regulation, load switches for waking up sensors or actuators utilizing the transferred power and circuitry for using surplus power for charging batteries or super capacitors.

Even though the power levels attained are considerable, especially for the case with conjugate matching, the output voltage levels are low (a couple hundred mV). This justifies the need for a boost converter rectifier. However, due to the internal workings of switching rectifiers, the boost conversion requires the use of an external inductor or transformer (such as in the EM8900), which adds to the footprint of the power

TABLE 3. Comparison with relevant state-of-the-art.

Reference	Material	Topology	Dimensions	Footprint	t_{piezo}	f	d	P_{out}	$I_{acoustic}$	R_{load}	η_{total}
				(mm^2)	(um)	(kHz)	(cm)	(uW)	(mW/cm^2)	(Ω)	(%)
[6]	PZT	Block	$1x1 \text{ mm}^2$	1	1400	1300	3	600	95	11	63
[37]	PZT	Diapraghm	1.6 mm radius	8.04	40	40.4	2	35	0.59	1300	74
[7]	PZT	Diaphragm	$2x2 \text{ mm}^2$	4	20	88	2	700	74.8	4300	24
[8]	PZT	1x7 PMUT array	$500 x 250 \text{ um}^2$	2.06^{-a}	2	330	2.3	0.085	0.067	50	14
This work	AlScN	20x20 PMUT array	46 um radius	12.25^{-a}	0.5	700	4	1000	100	13.8	38

^a Including unused chip free space between elements

transfer system. In other commercially-available integrated boost voltage conversion, regulation and battery charging management systems [32], [33], the integrated circuit is miniaturized but the inductor or transformer element still occupies areas of about $3 \times 3 \, mm^2$, limiting the implantability of the system.

Furthermore, these circuits operate from DC voltages, so diode bridge rectifiers are required. A test was performed, on the same power transfer setup, using a bridge composed of low voltage RF detector diodes [34] in which the low voltage output was successfully rectified. Other options for boosting of the voltage include switched capacitor voltage multipliers, after rectification. However, due to their simultaneous voltage boosting and capacitive reactance cancelling effect, the use of resonator-based matching networks for power transfer becomes appealing.

F. COMPARISON WITH THE STATE-OF-THE-ART

As mentioned in section I, several works demonstrate the performance of bulk piezoelectric transducers, operating in their thickness extensional mode, as ultrasonic power transfer receivers. [2], for example, provides an extensive comparison of many such implementations. However, the focus of this work is on a small form factor implementations and, particularly, on a PMUT structure. Therefore, the comparison with the state-of-the-art is constrained to piezoelectric diaphragm implementations and is summarized in table 3.

One exception is done for one example of a miniaturized PZT block used as receiver, as several works have used this approach for powering minute nodes capable of stimulation [3] and up-link of data from the node [35]. Such body of work also includes considerations for the design of the receivers [29] and proposes methods for enhancement of the power transfer through beam-forming towards the nodes [36].

[37] and [7] detail diaphragm structures with a relatively thick PZT layer and a correspondingly large radius to achieve low frequencies of operation, appealing to lowered attenuation in the medium. The fact that both structures have a comparable area and frequency of operation but very different efficiencies points out to the importance of optimization of the thickness ratio of the piezoelectric and passive layers for increased output.

[8] is an implementation with a piezoelectric thickness more comparable to the one used in the present work but attains a comparably lower efficiency, which could be related to the relationship between its element size and wavelength and the lack of a load optimization (a standard 50Ω value was used). The work, however, has valuable insight on compensation of the standing wave effect occurring in the space between the transmitter and receiver through frequency tuning.

Considering the wide range of geometries and dimensions surveyed as well as frequencies of operation and input acoustic intensities, the efficiency defined in section 3 served as a valuable figure of merit. Based on this value, the AlScN implementation is competitive while utilizing a thin piezoelectric layer, and offering the possibility of integration in CMOS-processing and higher bio-compatibility. The output power value is also considerably high for the matched case, even though the performance without matching is quite sufficient for powering of implantables.

IV. CONCLUSION

An AlScN PMUT array was designed and optimized, in terms of the effective electro-mechanical coupling coefficient of the transducer and its quality factor. The optimization was based on the ratio of the piezoelectric to passive layer thicknesses for a particular radius. Considerations on the trade-off between higher output power and increased directivity (decreasing tolerance to misalignment between transmitter and receiver) were explored.

Arrays based on AlN and Sc-doped AlN were fabricated and good quality of the piezoelectric film was confirmed. Sc doping of AlN PMUT demonstrated a sensible enhancement of the transmission performance from a reference transmitter to the PMUT array. From the impulse response measurements, a 25dB transmission increase was measured with Sc versus the case with no doping. A significant bandwidth, normalized to the center frequency, of 77% also proved to be another desirable characteristic of the material for implantable communication applications.

Load optimization experiments matched closely the simulated outputs, and conjugate matching was proven to increase the transferred power significantly. Experiments were also conducted to assess the possibility of utilizing resonators, with a high quality factor, to perform conjugate matching of the capacitive load the PMUT array inherently presents. Even though the power levels attained do not matched the ones available with inductor matching, the use of resonators offered a voltage boosting effect, desirable for rectification

of the voltage without requiring circuitry such as boost converters.

For the optimal load case, output power levels of 4.5 and $0.5mW_{rms}$ were obtained for an incident sound intensity $(I_{acoustic})$ of $500mW/cm^2$ for cases with and without matching, respectively. The performance values were compared with relevant state-of-the-art and the conversion efficiency of the receiver was used to benchmark different receivers. A competitive performance, plus a practical demonstration of voltage rectification through a COTS boost converter, set this work as an enabling demonstration towards utilizing AlScN PMUT arrays for powering and recharging in implantable electronics applications.

ACKNOWLEDGMENT

The authors would like to thank the staff of the George J. Kostas Nanoscale Technology and Manufacturing Research Center for assistance in device fabrication.

REFERENCES

- K. Agarwal, R. Jegadeesan, Y. Guo, and N. Thakor, "Wireless power transfer strategies for implantable bioelectronics," *IEEE Rev. Biomed.* Eng., vol. 10, pp. 136–161, 2017.
- [2] H. Basaeri, D. B. Christensen, and S. Roundy, "A review of acoustic power transfer for bio-medical implants," *Smart Mater. Struct.*, vol. 25, no. 12, 2016, Art. no. 123001.
- [3] M. J. Weber, A. Bhat, T. C. Chang, J. Charthad, and A. Arbabian, "A miniaturized ultrasonically powered programmable optogenetic implant stimulator system," in *Proc. IEEE Topical Conf. Biomed. Wireless Technol., Netw.*, Sens. Syst. (BioWireleSS), Jan. 2016, pp. 12–14.
- [4] D. Seo et al., "Wireless recording in the peripheral nervous system with ultrasonic neural dust," *Neuron*, vol. 91, no. 3, pp. 529–539, Apr. 2016.
- [5] S. Sonmezoglu, J. R. Fineman, E. Maltepe, and M. M. Maharbiz, "Monitoring deep-tissue oxygenation with a millimeter-scale ultrasonic implant," *Nature Biotechnol.*, vol. 39, no. 7, pp. 855–864, Jul. 2021.
- [6] J. Charthad, M. J. Weber, T. C. Chang, and A. Arbabian, "A mm-sized implantable medical device (IMD) with ultrasonic power transfer and a hybrid Bi-directional data link," *IEEE J. Solid-State Circuits*, vol. 50, no. 8, pp. 1741–1753, Aug. 2015.
- [7] H. Basaeri, Y. Yu, D. Young, and S. Roundy, "Acoustic power transfer for biomedical implants using piezoelectric receivers: Effects of misalignment and misorientation," *J. Micromech. Microeng.*, vol. 29, no. 8, Aug. 2019, Art. no. 084004.
- [8] Q. Shi, T. Wang, and C. Lee, "MEMS based broadband piezoelectric ultrasonic energy harvester (PUEH) for enabling self-powered implantable biomedical devices," Sci. Rep., vol. 6, no. 1, pp. 1–10, Jul. 2016.
- [9] B. Herrera, F. Pop, C. Cassella, and M. Rinaldi, "AlN PMUT-based ultrasonic power transfer links for implantable electronics," in *Proc. 20th Int. Conf. Solid-State Sensors, Actuat. Microsyst. Eurosensors XXXIII* (TRANSDUCERS EUROSENSORS XXXIII), Jun. 2019, pp. 861–864.
- [10] R. H. Olsson, Z. Tang, and M. D'Agati, "Doping of aluminum nitride and the impact on thin film piezoelectric and ferroelectric device performance," in *Proc. IEEE Custom Integr. Circuits Conf. (CICC)*, Mar. 2020, pp. 1–6.
- [11] M. Akiyama, K. Umeda, A. Honda, and T. Nagase, "Influence of scandium concentration on power generation figure of merit of scandium aluminum nitride thin films," Appl. Phys. Lett., vol. 102, no. 2, 2013, Art. no. 021915.
- [12] Q. Wang, Y. Lu, S. Mishin, Y. Oshmyansky, and D. A. Horsley, "Design, fabrication, and characterization of scandium aluminum nitride-based piezoelectric micromachined ultrasonic transducers," *J. Microelectromech. Syst.*, vol. 26, no. 5, pp. 1132–1139, Oct. 2017.
- [13] E. Ledesma, I. Zamora, A. Uranga, and N. Barniol, "9.5% scandium doped ALN PMUT compatible with pre-processed CMOS substrates," in Proc. IEEE 34th Int. Conf. Micro Electro Mech. Syst. (MEMS), Jan. 2021, pp. 887–890.

- [14] G. Giribaldi, B. H. Soukup, P. Simeoni, L. Colombo, and M. Rinaldi, "Matching network-boosted 36% scaln pmut linear array," in *Proc. IEEE* 35th Int. Conf. Micro Electro Mech. Syst. Conf. (MEMS), Jan. 2022, pp. 251–254.
- [15] B. Herrera, G. Giribaldi, M. Pirro, L. Colombo, and M. Rinaldi, "Wireless ultrasonic power transfer for implantables via scandium-doped aln pmut arrays," in *Proc. IEEE 35th Int. Conf. Micro Electro Mech. Syst. Conf.* (MEMS), Jan. 2022, pp. 837–840.
- [16] M. Pirro, B. Herrera, M. Assylbekova, G. Giribaldi, L. Colombo, and M. Rinaldi, "Characterization of dielectric and piezoelectric properties of ferroelectric AlScN thin films," in *Proc. IEEE 34th Int. Conf. Micro Electro Mech. Syst. (MEMS)*, Jan. 2021, pp. 646–649.
- [17] P. Muralt et al., "Piezoelectric micromachined ultrasonic transducers based on PZT thin films," *IEEE Trans. Ultrason., Ferroelectr., Freq. Control*, vol. 52, no. 12, pp. 2276–2288, Dec. 2005.
- [18] A. L. des Etangs-Levallois et al., "A converging route towards very high frequency, mechanically flexible, and performance stable integrated electronics," J. Appl. Phys., vol. 113, no. 15, Apr. 2013, Art. no. 153701.
- [19] J. J. Bernstein et al., "Micromachined high frequency ferroelectric sonar transducers," *IEEE Trans. Ultrason., Ferroelectr., Freq. Control*, vol. 44, no. 5, pp. 960–969, Sep. 1997.
- [20] K. Smyth and S.-G. Kim, "Experiment and simulation validated analytical equivalent circuit model for piezoelectric micromachined ultrasonic transducers," *IEEE Trans. Ultrason., Ferroelectr., Freq. Control*, vol. 62, no. 4, pp. 744–765, Apr. 2015.
- [21] X. Jiang et al., "Monolithic ultrasound fingerprint sensor," *Microsyst. Nanoeng.*, vol. 3, no. 1, pp. 1–8, Nov. 2017.
- [22] L. W. Schmerr, Jr., Fundamentals of Ultrasonic Phased Arrays, vol. 215. Switzerland: Springer, 2014.
- [23] C. H. Sherman and J. L. Butler, *Transducers and Arrays for Underwater Sound*, vol. 4. New York, NY, USA: Springer, 2007.
- [24] L. Colombo, A. Kochhar, G. Vidal-Alvarez, and G. Piazza, "High-figure-of-merit X-cut lithium niobate MEMS resonators operating around 50 MHz for large passive voltage amplification in radio frequency applications," *IEEE Trans. Ultrason., Ferroelectr., Freq. Control*, vol. 67, no. 7, pp. 1392–1402, Jul. 2020.
- [25] J. Segovia-Fernandez et al., "Monolithic AlN MEMS-CMOS resonant transformer for wake-up receivers," in *Proc. IEEE Int. Ultrason. Symp.* (IUS), Sep. 2017, pp. 1–4.
- [26] B. H. Soukup, P. Simeoni, G. Giribaldi, L. Colombo, and M. Rinaldi, "MEMS resonator matching network for high-sensitivity scaln pmutbased ultrasound receivers," in *Proc. Hilton Head Solid-State Sensors*, Actuat. Microsystems Workshop, 2022, pp. 376–378.
- [27] Em8900-PMU DC Energy Harvesting Controller. Accessed: May 5, 2022. [Online]. Available: https://www.emmicroelectronic.com/product/pmu-dc-energy-harvesting-controller/em8900
- [28] PMUTS Layout and Analysis Tool. Accessed: May 10, 2022. [Online]. Available: https://github.com/simeonipietro/pMUTs_Layout_and_ Analysis_Tool
- [29] T. C. Chang, M. J. Weber, J. Charthad, S. Baltsavias, and A. Arbabian, "End-to-end design of efficient ultrasonic power links for scaling towards submillimeter implantable receivers," *IEEE Trans. Biomed. Circuits Syst.*, vol. 12, no. 5, pp. 1100–1111, Oct. 2018.
- [30] A. S. Rekhi, B. T. Khuri-Yakub, and A. Arbabian, "Wireless power transfer to millimeter-sized nodes using airborne ultrasound," *IEEE Trans. Ultra*son., Ferroelectr., Freq. Control, vol. 64, no. 1, pp. 1526–1541, Oct. 2017.
- [31] Em8502—PMU & DC Energy Harvesting Controller. Accessed: May 5, 2022. [Online]. Available: https://www.emmicroelectronic.com/ product/pmu-dc-energy-harvesting-controller/em8502
- [32] Ultralow Power Energy Harvester PMU With MPPT and Charge Management. Accessed: May 5, 2022. [Online]. Available: https://www. analog.com/en/products/adp5092.html?doc=ADP5091-1-EVALZ-ADP5092-1-EVALZ-UG-967.pdf#product-overview
- [33] Ultra-Low Voltage Energy Harvester and Primary Battery Life Extender. Accessed: May 5, 2022. [Online]. Available: https://www.analog.com/media/en/technical-documentation/data-sheets/3107f.pdf
- [34] Surface-Mount Mixer and Detector Schottky Diodes. Accessed: May 5, 2022. [Online]. Available: https://www.skyworksinc.com/-/media/ SkyWorks/Documents/Products/201-300/Surface_Mount_Schottky_ Diodes_200041AG.pdf
- [35] M. M. Ghanbari et al., "17.5 A 0.8 mm³ ultrasonic implantable wireless neural recording system with linear AM backscattering," in *IEEE Int. Solid-State Circuits Conf. (ISSCC) Dig. Tech. Papers*, Feb. 2019, pp. 284–286.

- [36] M. L. Wang, T. C. Chang, and A. Arbabian, "Ultrasonic implant localization for wireless power transfer: Active uplink and harmonic backscatter," in *Proc. IEEE Int. Ultrason. Symp. (IUS)*, Oct. 2019, pp. 818–821.
- [37] Q. He, J. Liu, B. Yang, X. Wang, X. Chen, and C. Yang, "MEMS-based ultrasonic transducer as the receiver for wireless power supply of the implantable microdevices," *Sens. Actuators A, Phys.*, vol. 219, pp. 65–72, Nov. 2014.



BERNARD HERRERA (Member, IEEE) received the B.Sc. degree in electrical engineering from the Universidad San Francisco de Quito, Ecuador, in 2011, and the M.Sc. degree in electrical and computer engineering from Northeastern University in 2017, where he is currently pursuing the Ph.D. degree with the Northeastern Sensors and Nano Systems Laboratory led by Prof. Matteo Rinaldi. During his studies, he did an exchange year at the University of Illinois at

Urbana-Champaign, USA, where he also performed as a Research Assistant. He then joined the Universidad San Francisco de Quito as an Instructor and a Researcher. His research interests include piezoelectric micromachined ultrasonic transducers with intra-body and underwater applications.



PIETRO SIMEONI (Member, IEEE) received the B.S. degree in physics engineering and the M.S. degree in nanotechnologies for ICTs from the Politecnico di Torino, Turin, Italy, in 2014 and 2016, respectively, and the Ph.D. degree from Carnegie Mellon University, in 2021, where his research focused on airborne ultrasonic communication for low-power wake-up applications. Currently, he is with the Electrical and Computer Engineering Department, Northeastern University.

His research interests include device and system level development of piezoelectric electromechanical sensing platforms. He is the 2019 Marsha and Philip Dowd Graduate Fellow.



GABRIEL GIRIBALDI (Student Member, IEEE) received the B.Sc. degree in physical engineering from the Politecnico di Torino, Turin, in 2018, and the joint M.Sc. degree in micro and nanotechnologies for integrated systems from the Politecnico di Torino and the Institut Nationale Polytechnique PHELMA, Grenoble, in 2020. He is currently pursuing the Ph.D. degree with Northeastern University, with research focus on piezoelectric MEMS resonators for X-band and beyond passive filters

and ultrasound transducers for the Internet of Things applications.



LUCA COLOMBO (Member, IEEE) received the B.Sc. and M.Sc. degrees in mechanical engineering from the Politecnico di Milano, Milan, Italy, in 2013 and 2015, respectively, and the Ph.D. degree in electrical and computer engineering from Carnegie Mellon University, Pittsburgh, PA, USA, in 2019. He is currently an Associate Research Scientist at Northeastern University, Boston, MA, USA. His research interests include RF MEMS for ultra-low-power applications.



MATTEO RINALDI (Senior Member, IEEE) received the Ph.D. degree in electrical and systems engineering from the University of Pennsylvania, Philadelphia, PA, USA, in December 2010. He was a Postdoctoral Researcher with the University of Pennsylvania in 2011. In January 2012, he joined the Electrical and Computer Engineering Department, Northeastern University, Boston, MA, USA, as an Assistant Professor. He is currently an Associate Professor with the Electrical

and Computer Engineering Department, Northeastern University, and the Director of the Northeastern SMART Center, a university research center that, by fostering partnership between university, industry, and government stakeholders, aims to conceive and pilot disruptive technological innovation in devices and systems capable of addressing fundamental technology gaps in several fields, including the Internet of Things (IoT), 5G, quantum engineering, digital agriculture, robotics, and healthcare. His group has been actively working on experimental research topics and practical applications to ultra-low power MEMS/NEMS sensors (infrared, magnetic, chemical, and biological, plasmonic micro- and nano-electromechanical devices, medical microsystems and implantable microdevices for intra-body networks, reconfigurable radio frequency devices and systems, phase change material switches, and 2-D material enabled micro- and nano-mechanical devices). His group's research was supported by several Federal grants (including DARPA, Advanced Research Projects Agency-Energy, National Science Foundation (NSF), and Department of Homeland Security), the Bill and Melinda Gates Foundation and the Keck Foundation with funding of over \$14 M since 2012. He has coauthored more than 130 publications in the aforementioned research areas. He also holds eight patents and more than ten device patent applications in the field of MEMS/NEMS. He was a recipient of the IEEE Sensors Council Early Career Award in 2015, the NSF CAREER Award in 2014, and the DARPA Young Faculty Award in the class of 2012. He received the Best Student Paper Award at the 2009, 2011, 2015 (with his student), and 2017 (with his student) IEEE International Frequency Control Symposiums, the Outstanding Paper Award at the 18th International Conference on Solid-State Sensors, Actuators and Microsystems, Transducers 2015 (with his student), and the Outstanding Paper Award at the 32nd IEEE International Conference on Micro Electro Mechanical Systems, MEMS 2019 (with his student).

260 VOLUME 2. 2022